Supporting Information for: Consistent prokaryotic successional dynamics across contrasting phytoplankton blooms

Markel Gómez-Letona[1,2]*, Javier Arístegui[1]*, Ulf Riebesell[3], Marta Sebastián[1,4]

[1] Instituto de Oceanografía y Cambio Global, Universidad de Las Palmas de Gran Canaria (ULPGC), Las Palmas, Spain

[2] Instituto de Investigacións Mariñas (IIM), CSIC, Vigo, Spain

[3] Biological Oceanography, Marine Biogeochemistry, GEOMAR Helmholtz Centre for Ocean Research Kiel, Kiel, Germany

[4] Department of Marine Biology and Oceanography, Institut de Ciències del Mar (ICM), CSIC, Barcelona, Spain

* Corresponding authors:

Markel Gómez-Letona: markel.gomez101@alu.ulpgc.es

Javier Arístegui: javier.aristegui@ulpgc.es

List of contents

Supplementary methods

Supplementary figures

References

Supplementary methods

Single cell translational activity of prokaryotes

The single-cell translational (i.e., protein-synthesising) activity of prokaryotes was assessed by BioOrthogonal Non-Canonical Amino acid Tagging (BONCAT) following Leizeaga et al. (2017). For each sampling time and mesocosm two replicates and a control (9 mL each) were incubated with L-Homopropargylglycine (HPG, a surrogate of the methionine amino acid) at a final concentration of 1 µM for 2h at in situ temperature. The control was fixed with paraformaldehyde prior to HPG addition at a final concentration of 2% (v/v), and replicates were likewise fixed to finalise incubations, after which they were left overnight at 4°C. Samples were then gently filtered through polycarbonate filters with a pore size of 0.2 µm (Whatman Nuclepore). Filters were washed thrice with sterile ultrapure water, labelled and stored at -80°C until further processing.

Filters were subsequently processed by submerging them in a pre-boiled agarose solution (0.1 % w/w) to ensure cell attachment to the filters and avoid cell loss during downstream processing. After drying the filters at 37°C they were dehydrated with ethanol (96%, v/v). Cells were then permeabilised with 1) freshly prepared lysozyme solution (10 $mg \cdot mL^{-1}$; 0.05 M EDTA, 0.1 M Tris-HCL) for 1h at 37°C and 2) achromopeptidase (60 $U \cdot mL^{-1}$; 0.01 M NaCl, 0.01 M Tris-HCl, pH 8.0) for 30' at 37°C (Sekar et al. 2003). Filters were subsequently washed with sterile ultrapure water and ethanol (96%, v/v). Next, Cu(I)-catalyzed click chemistry was performed. A dye premix was prepared with 10 µL of 20 mM copper sulfate solution ($CuSO_4 \cdot 5H_2O$), 8 µL of 1 mM Alexa594 azide dye (ThermoFisher) and 20 µL of 50 mM Tris[(1-hydroxypropyl-1H-1,2,3-triazol-4-yl)methyl]amine (THPTA), and left to react in the dark at room temperature for 3'. A solution combining 100 µL of freshly prepared 10 mM sodium ascorbate solution in phosphate buffered saline (PBS), 100 µL of freshly prepared 10 mM aminoguanidine hydrochloride solution in PBS, and 1.77 mL of PBS solution was prepared in the meantime. For the click reaction mix, the dye premix and the PBS-ascorbate-aminoguanidine solution were combined, gently inverting the tube twice to ensure homogenisation. The click reaction mix was then quickly added to a 1.5 mL tube containing a triangular filter piece of each sample, filling the entire tube and its cap to avoid air bubbles and hence maintain reducing conditions. Furthermore, after closing the tube the cap was sealed with parafilm to ensure no air exchange happened. The tube was placed in the dark at room temperature for 30' to let the click reaction take place. Filters were subsequently washed thrice with PBS and once each with ethanol at 50, 70 and 96% (v/v). A final 1h wash with a solution of PBS:ethanol (1:1) was performed to reduce the background fluorescence signal. Filters were counterstained with 4′,6-diamidino-2-phenylindole (DAPI; 1 $\mu g \cdot mL^{-1}$ final concentration), placed in microscope slides with antifading reagent (77% glycerol, 15% VECTASHIELD and 8% 20x PBS) and covered with glass covers.

Image acquisition to quantify translationally active cells was done in black and white with a Zeiss Axio Imager.Z2m Epifluorescence Microscope connected to a Zeiss camera (AxioCam MRm, Carl Zeiss MicroImaging, S.L., Barcelona, Spain) at 630× magnification, along with the AxioVision software. A Colibri LED light source (Carl Zeiss) with multiple light-emitting diodes was used, capturing all images at excitation of both 1) 385 nm for DAPI and 2) 590 nm for Alexa594, adjusting exposure time to optimise cell detection. Images analysis to quantify total (DAPI) and translationally active (BONCAT+) cells was carried out with the ACMEtool software.

Bulk activity of prokaryotes

Bulk prokaryotic activity was estimated as prokaryotic heterotrophic production (PHP) by means of ^{3}H-leucine incorporation using the centrifugation method (Smith and Azam 1992). ^{3}H-leucine (Perkin-Elmer, specific activity 160 Ci mmoL^{-1}) was added to quadruplicate 1 mL subsamples (final concentration: 20 nmol L^{-1}) in microcentrifuge tubes. Blanks were established by adding 100 µL of 50% trichloroacetic acid (TCA) to duplicate empty microcentrifuge tubes 15 min prior to radioisotope addition. Subsamples and blanks were incubated at in situ temperature (~21 ± 1°C) in the dark for 2 h. Incubations were stopped by adding 100 µL ice-cold 50% TCA to the subsamples, and all tubes were kept at –20°C until centrifugation at 12000 rpm for 20 min. After removing the supernatant, 1 mL of scintillation cocktail (Ultima Gold XR) was added to the tubes and they were stored in darkness for 24 h. Subsequently, incorporated radioactivity was determined on a scintillation counter (Beckmann LS-6500). The mean disintegrations per minute (DPM) of the TCA-killed blanks were removed from the mean DPM of the respective samples and the resulting DPM value was converted into leucine incorporation rate. PHP was calculated using a conservative theoretical conversion factor of 1.55 kg C moL-1 Leu assuming no internal isotope dilution (Kirchman 1993).

Inorganic nutrients

Subsamples of 250-500 mL were collected into polypropylene bottles to measure nitrate (NO_3^-), nitrite (NO_2^-), ammonium (NH_4^+), phosphate (PO_4^{3-}) and silicic acid ($Si(OH)_4$). These subsamples were filtered through glass fibre filters with a pore size of 0.45 µm (Sterivex, Merck, Darmstadt, Germany) and inorganic nutrient concentrations were quantified spectrophotometrically on a five-channel continuous flow analyser (QuAAtro AutoAnalyzer, SEAL Analytical Inc., Mequon, USA).

Chl a

Samples for bulk Chl *a* (0.3-1 L) were filtered through pre-combusted glass fibre filters (0.7 µm pore size, Whatman GF/F, Maidstone, UK), and these were stored at –80°C in cryovials until analysis. To extract pigments, 0.5 mm glass beads and 1.3 mL of 100% high-performance liquid chromatography (HPLC)-grade acetone (Baker 8142, Avantor, Radnor, PA, United States) were added to samples. The extraction was performed in a homogenizer (Precellys, Montigny-le-Bretonneux, France). The mixture was centrifuged for 10 min at 10000 rpm, 4°C. The supernatant was removed with a syringe and filtered through a PTFE filter (0.2 µm pore size, VWR International GmbH, Darmstadt, Germany). Chl *a* (among other photosynthetic pigments) was measured by means of an HPLC Ultimate 3,000 (Thermo Scientific GmbH, Schwerte, Germany).

Samples for fractionated Chl *a* (500 mL) were sequentially filtered through a set of three polycarbonate filters with pore size of 20 µm, 2 µm and 0.2 µm (DHI GVS 20 µm, Hørsholm, Denmark; Whatman Nuclepore 2 µm and 0.2 µm, Maidstone, UK). Filters were placed in cryovials and stored at –20°C until analysis. Pigment extraction was carried out by submerging filters in 10 ml of acetone (90%) for 24 hours at 4°C. The extract was analysed on a Turner Design AU-10 fluorometer (San Jose, USA) according to Welschmeyer (1994).

Particulate organic matter

Samples for elemental analysis of particulate organic matter were filtered through pre-combusted glass fibre filters (0.7 µm pore size, Whatman GF/F, Maidstone, UK). Filters for particulate organic carbon (POC) and nitrogen (PON) were acidified for ~2 h to remove inorganic carbon, using 1 mol L^{-1} HCl, and dried over night at 60°C in pre-combusted glass

petri dishes. Filters for total particulate carbon (TPC) were dried without prior acidification. All filters were packed in tin cups (8 × 8 × 15 mm, LabNeed GmbH, Nidderau, Germany) and were measured on a CN analyser (Euro EA-CN, HEKAtech) according to Sharp (1974). If obtained POC concentrations were more than 10% higher than those of TPC (due to handling or measurement errors), POC was set to be equal to the TPC value (i.e., assuming that no particulate inorganic carbon was present).

Diatom community composition

Diatoms were identified and counted using a Zeiss Axiovert 100 microscope (Carl Zeiss, Germany) following Utermöhl (1931).

Dissolved organic matter characterisation

Dissolved organic matter (DOM) was quantified as dissolved organic carbon (DOC), nitrogen (DON) and phosphorus (DOP). DOC samples (10 mL) were stored in high density polyethylene bottles at –20°C until analysis. DOC measurements were performed with a Shimadzu TOC-5000 analyser (Sharp et al. 1993). Before the analysis, thawed samples were acidified with 50 µL of phosphoric acid (50%) and sparged with CO_2-free air for several minutes to remove inorganic carbon. To determine DOC concentrations, standard curves (30–200 µM) of potassium hydrogen phthalate were generated every day (Thomas et al. 1995), while reference material of deep sea water (42–45 µM C; D. A. Hansell laboratory, University of Miami) was also analysed daily. DON and DOP samples were also collected in high density polyethylene bottles and analysed according to Hansen and Koroleff (1999). 40 mL of the samples were filtered through cellulose acetate filters (0.45 µm pore size, Whatman). Total dissolved nitrogen and phosphorus were decomposed to phosphate and nitrate by adding one spoon of the oxidizing reagent Oxisolv (Merck) and cooking the solution for ~1h at 90-100°C. After cooling overnight, total dissolved nitrogen and phosphorus concentrations were measured spectrophotometrically on a continuous flow analyser (QuAAtro AutoAnalyzer, SEAL Analytical Inc., Mequon, USA). Triplicates of artificial seawater were (treated and measured each day) acted as blanks, and they were subtracted from the samples after averaging. DON and DOP concentrations were calculated as the remaining value after subtracting dissolved inorganic nitrogen and phosphate from total dissolved nitrogen and phosphorus, respectively.

The optical characterisation of DOM was performed by measuring its absorbance and fluorescence to determine chromophoric and fluorescent DOM (CDOM and FDOM, respectively). Absorbance spectra were measured using a USB2000+UV-VIS-ES Spectrometer (Ocean Optics) alongside a liquid waveguide capillary cell (World Precision Instruments) with a path length of 0.9982 m. Spectra extended across wavelengths between 178 nm and 878 nm and, for each sample, a blank was also measured using ultrapure Milli-Q water. Data processing was done in R (v. 4.1.2 (R Core Team 2021)) and consisted of three steps: 1) raw spectra were cropped between 250 and 700 nm, 2) blank spectra were subtracted from sample spectra, and 3) a baseline correction was performed by subtracting the average absorbance of each sample between 600 and 700 nm to the whole spectrum. No corrections were applied to the absorbance measurements to account for the potential effects that changes in salinity could have on the refractive index, as such effects were considered negligible for our equipment (see Catalá et al. 2018).

The processed absorbance spectra were transformed into absorption spectra following the definition of the Napierian absorption coefficient:

$$a_{\lambda} = 2.303 \times \frac{Abs_{\lambda}}{L}$$

where a_λ is the absorption coefficient at wavelength λ, Abs_λ the absorbance at wavelength λ, L the path length (in meters; here 0.9982 m) and *2.303* the factor to convert from decadic to natural logarithms.

The a_λ at 254 and 325 nm (a_{254} and a_{325}, respectively) were considered for this study as they are commonly used as proxies for CDOM concentration (Lønborg and Álvarez-Salgado 2014; Catalá et al. 2016, 2018). The slopes of the natural log-transformed absorption spectra for the wavelength ranges 275-295 nm and 350-400 nm ($S_{275-295}$ and $S_{350-400}$, respectively) were computed following Helms et al. (2008). These slopes (as well as their ratio, S_R) have been associated with changes in the molecular weight of CDOM, with higher slopes denoting lower average molecular weight (Helms et al. 2008, 2013), They have also been linked to the microbial reworking of organic matter in the ocean, decreasing values being associated with increased transformation of DOM by prokaryotes (Catalá et al. 2015, 2018).

FDOM was characterised with a Fluoromax-4 spectrofluorometer (Jobin Yvon Horiba), with an excitation range of 240-450 nm (10 nm increments) and an emission range of 300-560 nm (2 nm increments). Excitation and emission slit widths were set to 5 nm, and an integration time to 0.25 s. To correct for lamp spectral properties, measurements were carried out in signal-to-reference mode with instrument-specific excitation and emission corrections applied (Sc:Rc). Each sampling day three blanks were measured using ultrapure Milli-Q water (at the beginning, middle and end of the measurement process). Fluorescence measurements were collected into excitation-emission matrices and these were processed using the DOMFluor toolbox (v. 1.7 (Stedmon and Bro 2008)) in Matlab (R2017a). A weighted mean of the blanks was subtracted from each sample and excitation-emission matrices were normalized to the Raman area using the emission scan at 350 nm from blanks, calculating the area following the trapezoidal integration method (Lawaetz and Stedmon 2009). No inner-filter correction was performed because the average a_{250} value across all samples (2.120 ± 0.544 m^{-1}, mean ± sd; n = 208; max. = 3.4 m^{-1}), was lower than the threshold of 10 m^{-1} above which it is deemed necessary (Stedmon and Bro 2008). Rayleigh scatter bands of 1st (Em = Ex ± bandwidth) and 2nd (Em = 2·Ex ± 2·bandwith) orders were cut at each wavelength pair.

The resulting excitation-emission matrices (n = 175 after removing samples with errors) were analysed with a Parallel Factor (PARAFAC) analysis (Stedmon and Bro 2008) with the DOMFluor toolbox. The analysis yielded a five-component model (C1-C5) that was validated by split-half validation and random initialization. The fluorescence maximum of the components was recorded for each sample. Gómez-Letona et al. (2022) describe the characteristics of each component in detail and compares them to other fluorophores reported in the literature. Briefly, C1 and C5 presented excitation and emission spectra highly congruent with amino acid-/tryptophan-like fluorophores. C2 and C4 on the other hand were similar to previously identified humic-like components. C3 was discarded as it was likely related to fluorometer artifacts.

Supplementary figures

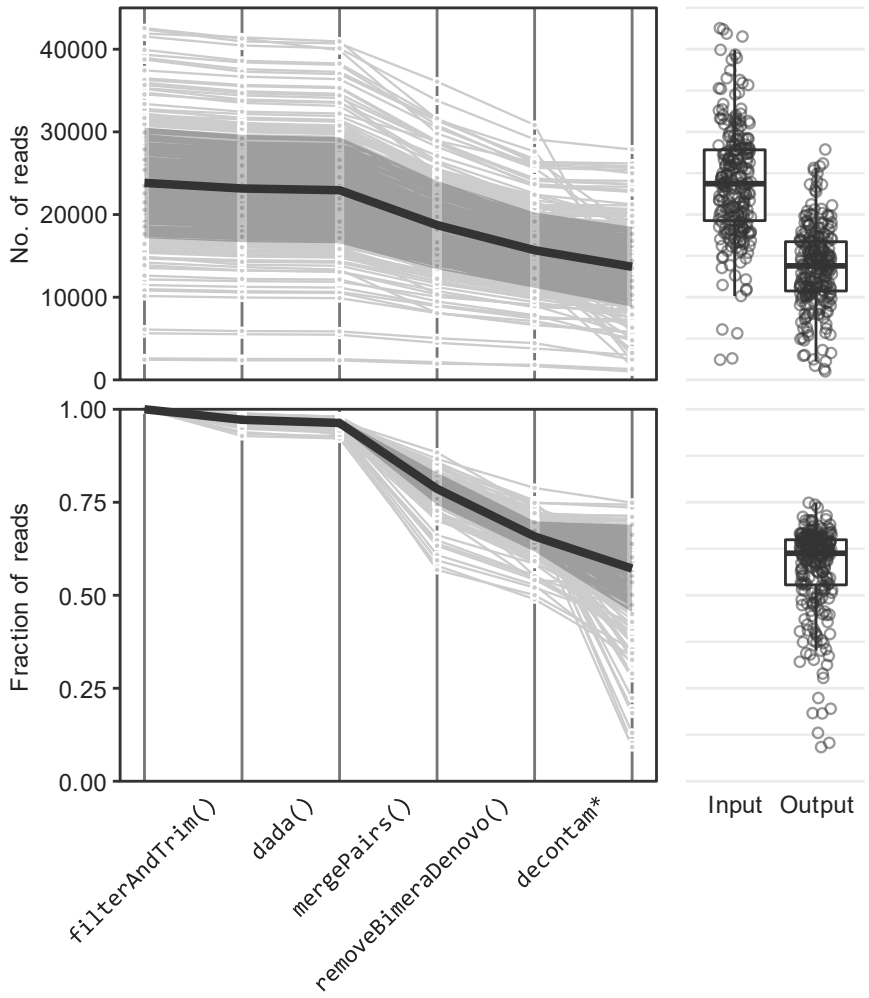

Fig. S1. Number of reads in absolute and relative (to the input) terms after each step of the processing of the sequencing data with *dada2*: 1) filtering and trimming of sequences, 2) core sample inference, 3) merging of paired reads and 4) chimera removal. The final *decontam** step includes the filtering out of ASVs identified as chloroplasts and mitochondria. Each grey line represents a sample, the black line represents their average value and the shaded grey area the standard deviation. The average fractions of reads preserved in each step relative to the previous one are: 0.97, 0.99, 0.82, 0.84 and 0.87. Boxplots display the distribution of read numbers before and after the processing pipeline. ↺

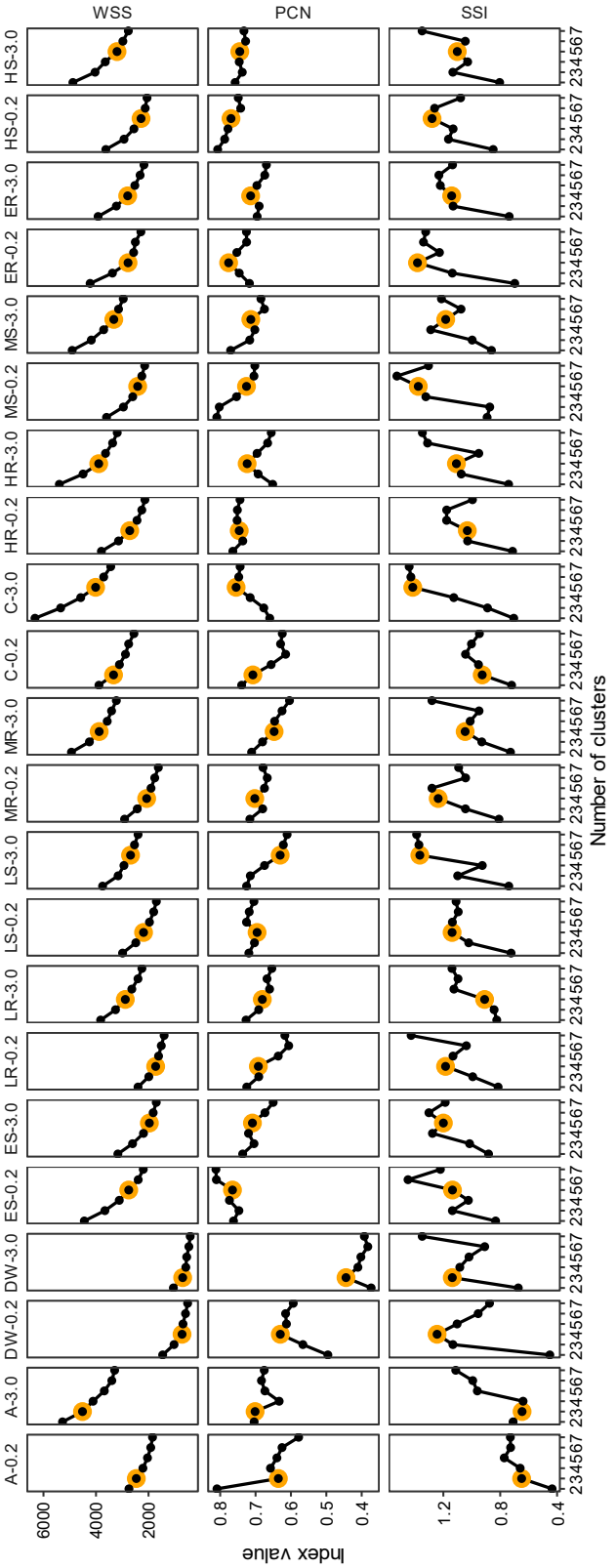

Figure S2. Results of the cluster selection indices, per treatment and size fraction. Within Cluster Sum of Squared Error (WSS), Normalized Partition Coefficient (PCN) and Simple Structure Index (SSI). The chosen cluster number is indicated with an orange circle. Treatments are denoted by the first letter of each word, along with the corresponding size fraction number. ↺

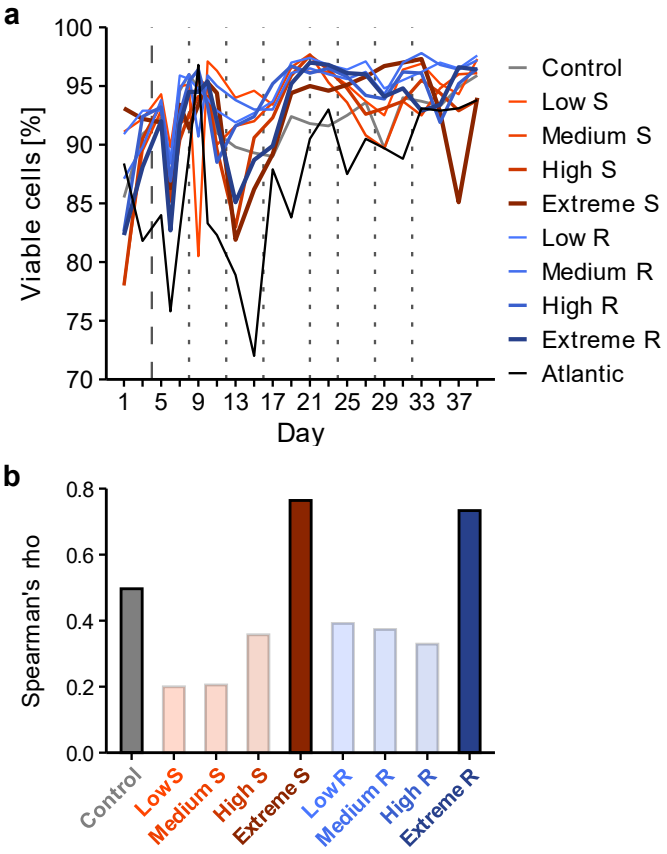

Figure S3. Viability of prokaryotic cells. a) Change in the percentage of viable cells (i.e., with intact cell membrane) within the prokaryotic community during the experiment. b) Correlation (Spearman's *rho*) between cell viability and (log_{10}-transformed) prokaryotic abundance. Bar transparency represents correlation significance (solid = p-value < 0.05; transparent otherwise). ↺

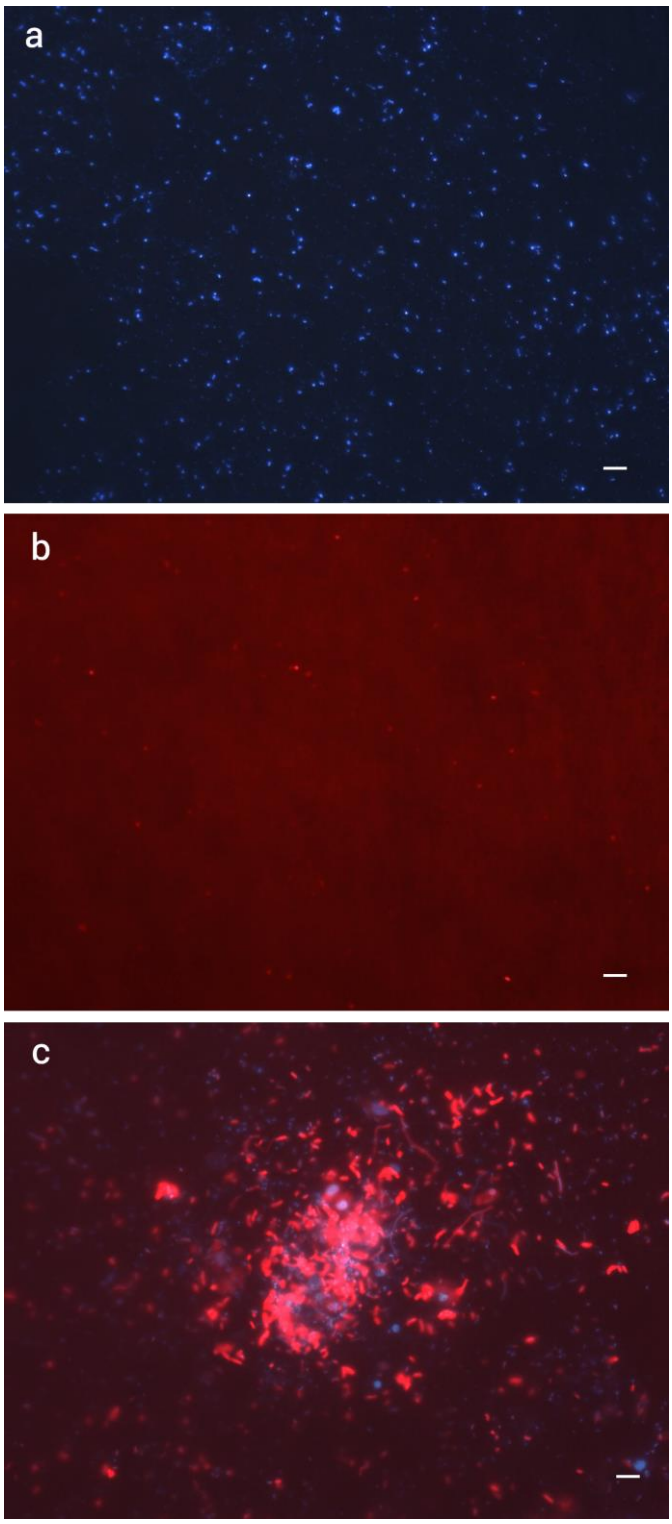

Figure S4. Single-cell protein synthesizing activity of prokaryotes in the extreme recurring (Extreme R) treatment. Images show a) day 3, signal of 4′,6-diamidino-2-phenylindole (DAPI; all cells, blue), b) corresponding Alexa594 (BONCAT+, protein-synthesising cells, red) signal for the same field, and c) day 13, combined DAPI and BONCAT+ signals. Scale bars (bottom right of each panel) represent 5 µm. ↺

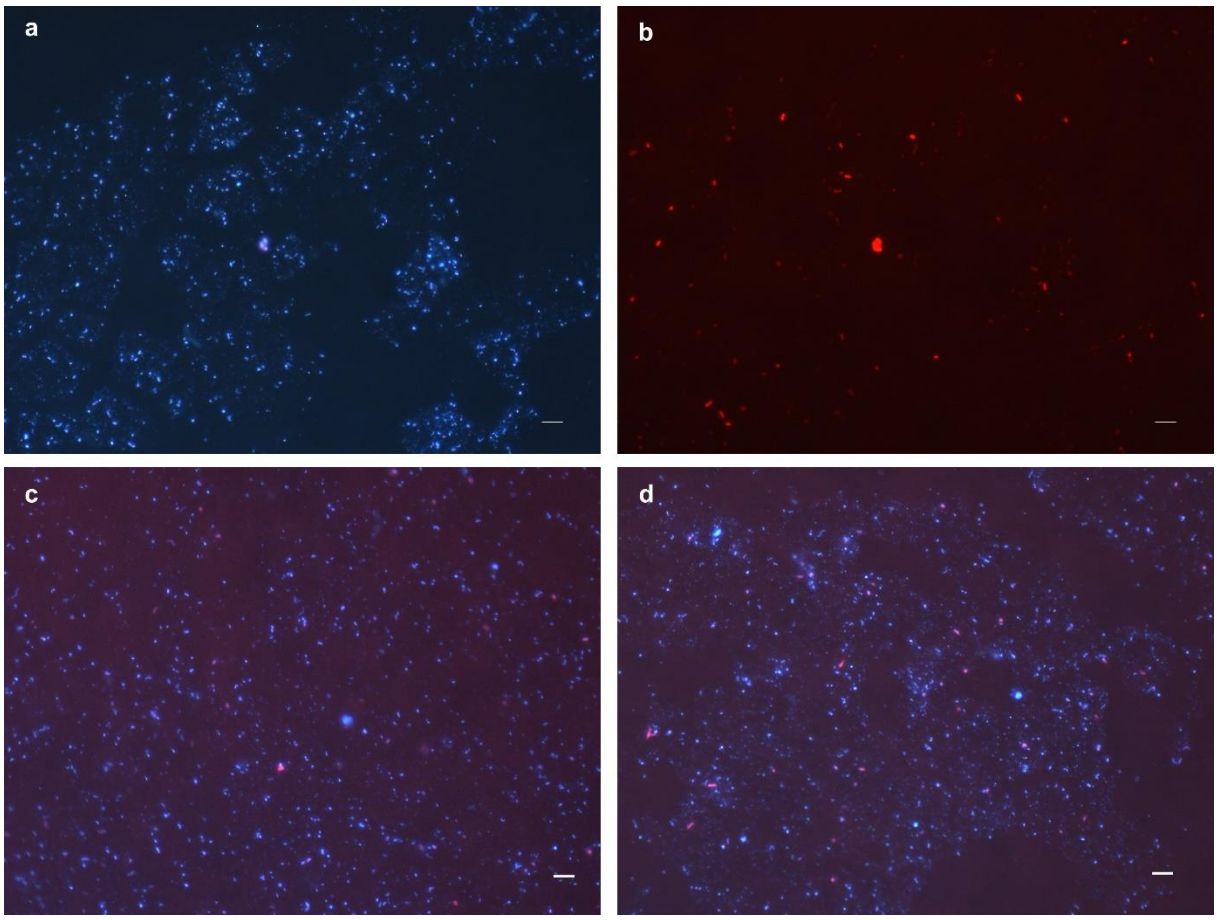

Figure S5. Single-cell protein synthesizing activity of prokaryotes in the Control mesocosm. Images show a) day 3, signal of 4′,6-diamidino-2-phenylindole (DAPI; all cells, blue), b) corresponding Alexa594 signal (BONCAT+, protein-synthesising cells, red) for the same field, c) day 13, combined DAPI and BONCAT+ signals and d) day 37, combined DAPI and BONCAT+ signals. Scale bars (bottom right of each panel) represent 5 µm. ↺

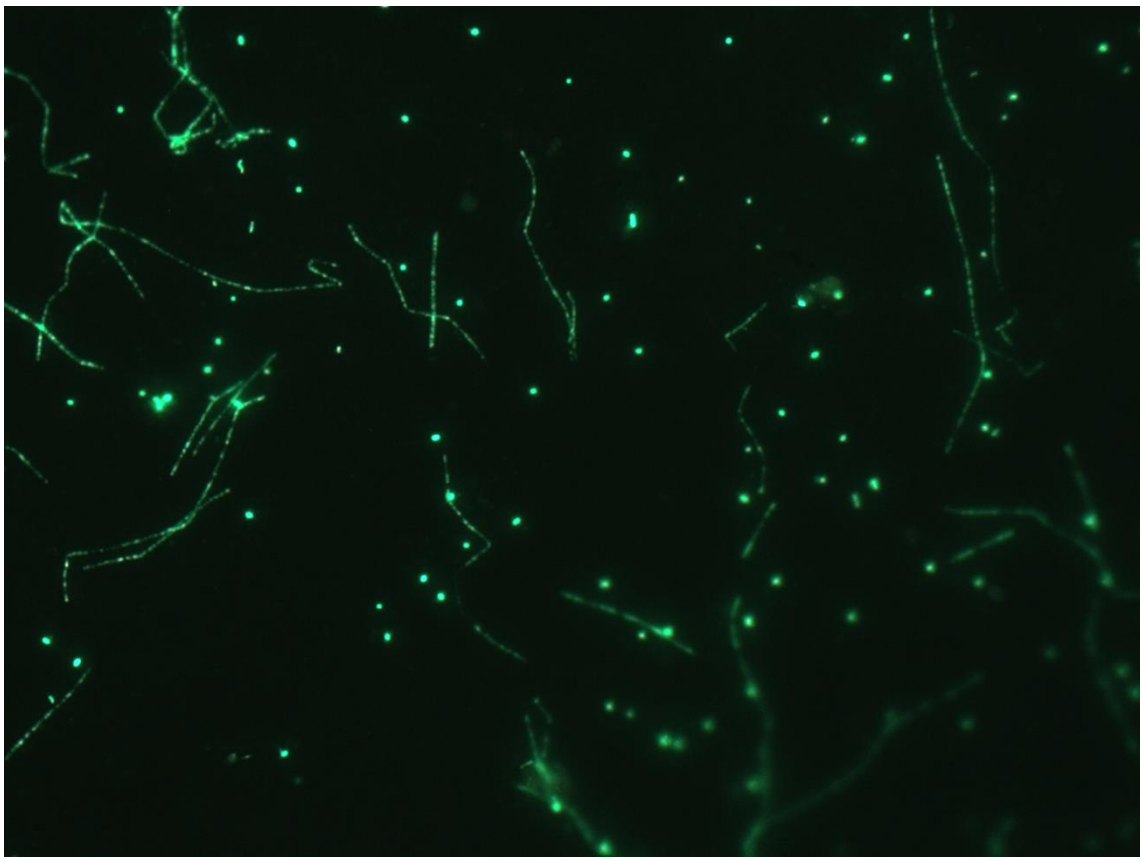

Figure S6. Identification of Bacteroidetes by means of Catalyzed Reporter Deposition Fluorescent in Situ Hybridization (CARD-FISH). In green, cells identified as Bacteroidetes in the Extreme R treatment on day 37. The highly active filamentous prokaryotes present in this mesocosm (Fig. 6d of the main text) are identified as Bacteroidetes. CARD-FISH was performed following Annelie et al. (2002). Samples were hybridized with the CF319a horseradish peroxidase-labelled probe, which targets many members of Bacteroidetes (Manz et al. 1996; Acinas et al. 2015). 55% formamide was added to the hybridization buffer to set appropriate hybridization conditions. Hybridization was performed overnight at 35°C. For amplification, a tyramide labelled with Alexa488 was used. Image acquisition was carried out as with BONCAT using a blue light source emitting at 470 nm. Image magnification: 630×. ↺

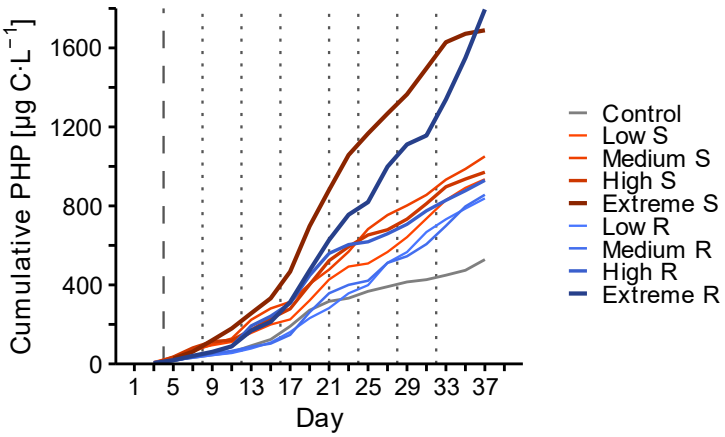

Figure S7. Cumulative prokaryotic heterotrophic production (PHP) during the experiment. ↺

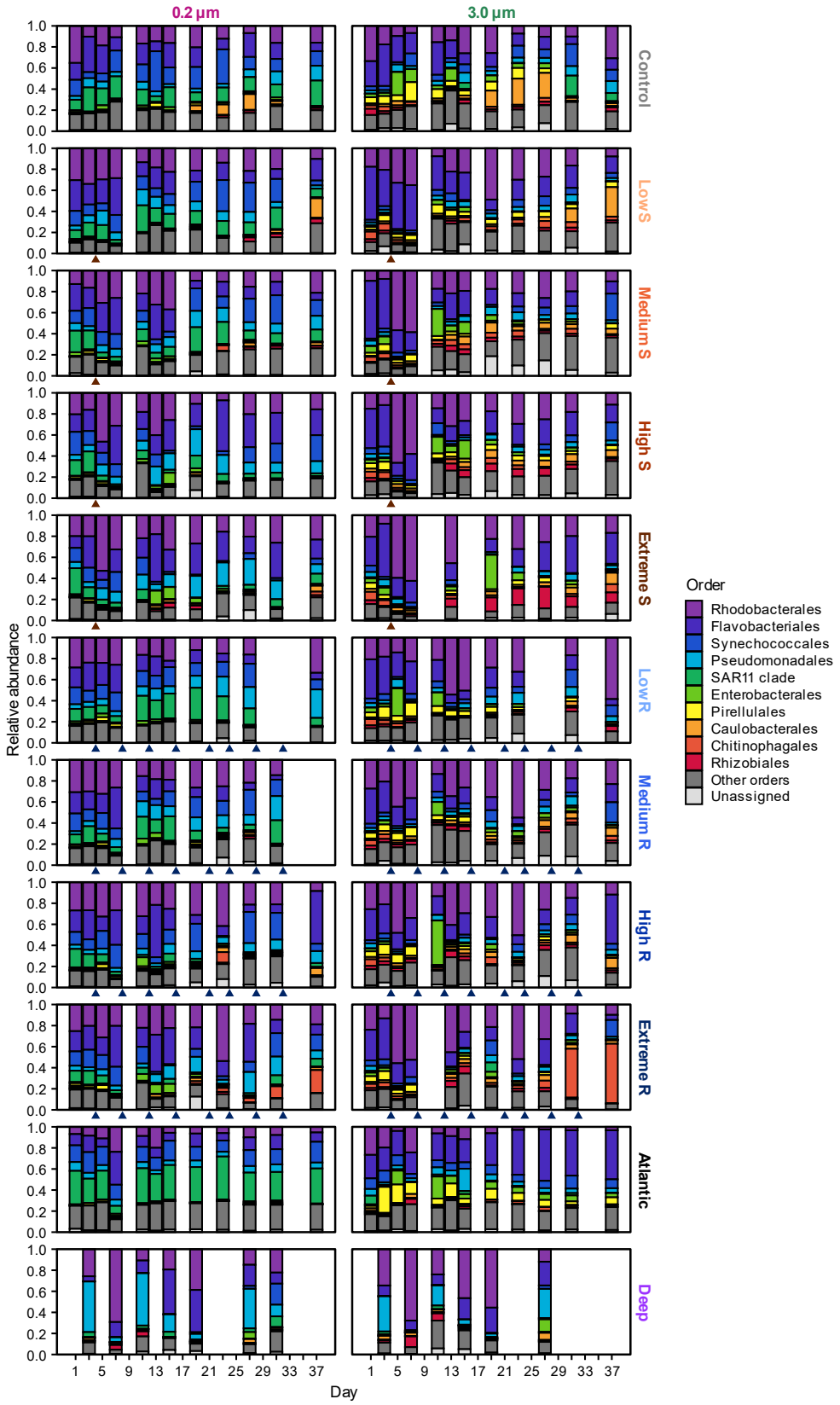

Fig. S8. Taxonomic composition of prokaryotic communities at the order level, per size fraction (0.2 µm and 3.0 µm) and treatment (*Deep* corresponds to the deep water bag). Triangles indicate deep water additions. ↺

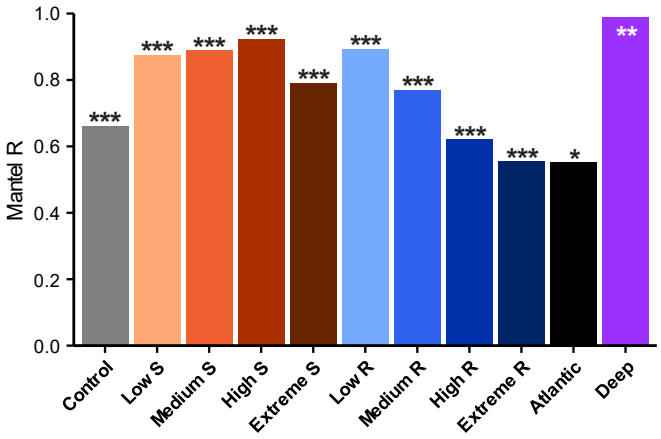

Fig. S9. Results of Mantel tests correlating changes in the composition of prokaryotic communities in both size fractions (0.2 µm and 3.0 µm), based on dissimilarity matrices (Euclidean distances) of the CLR-transformed ASV abundance table (Spearman method; tested with 9999 permutations, for the deep water the number of permutations was limited to 719 due to the reduced number of samples). Asterisks denote the significance of the results: $p < 0.05$ (*), $p < 0.01$ (**) and $p < 0.001$ (***). ↺

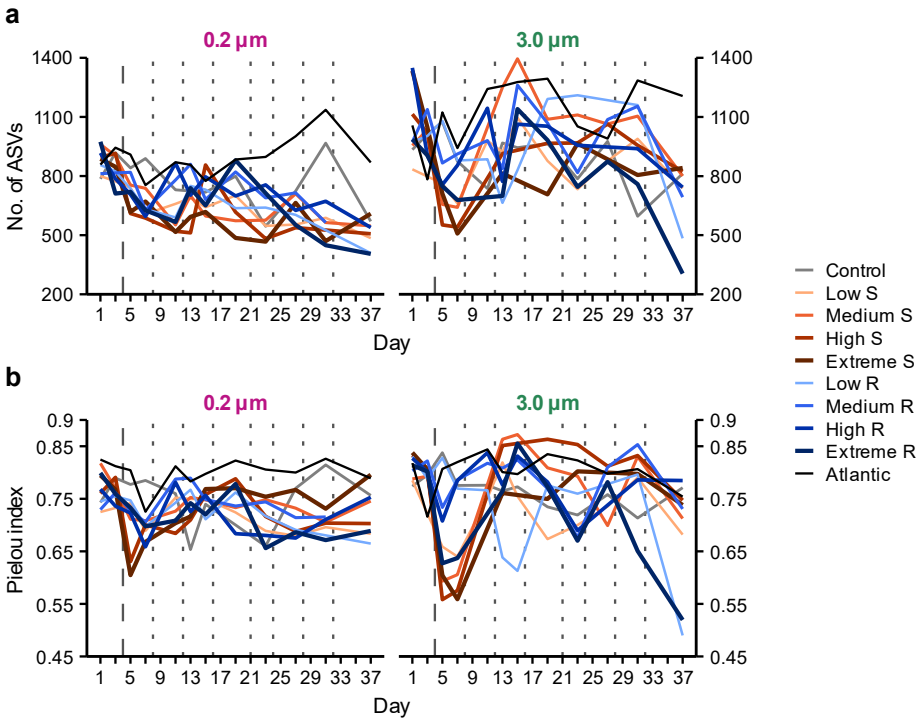

Figure S10. Temporal dynamics of prokaryotic diversity in the 0.2 µm (left panel) and 3 µm (right panel) size fractions. a) species richness as number of ASVs, and b) Pielou evenness index. Vertical lines represented deep water additions in the singular (dashed) and recurring treatments (dashed and dotted). ↺

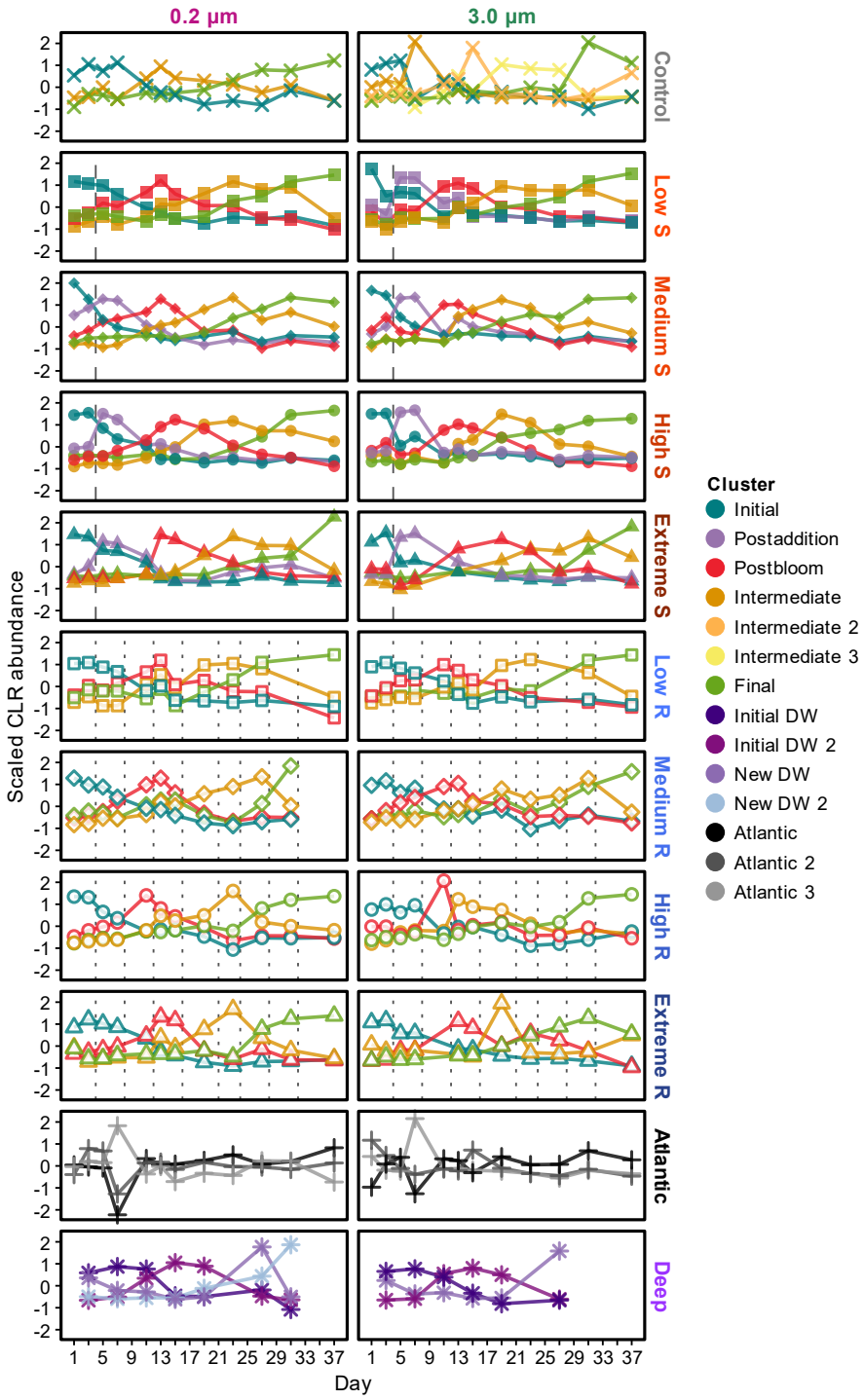

Figure S11. Temporal patterns of the cluster centroids obtained by fuzzy clustering of ASVs representing >0.1% in at least one sample (within each treatment). ASVs were assigned to the cluster in which they displayed the highest membership. ↺

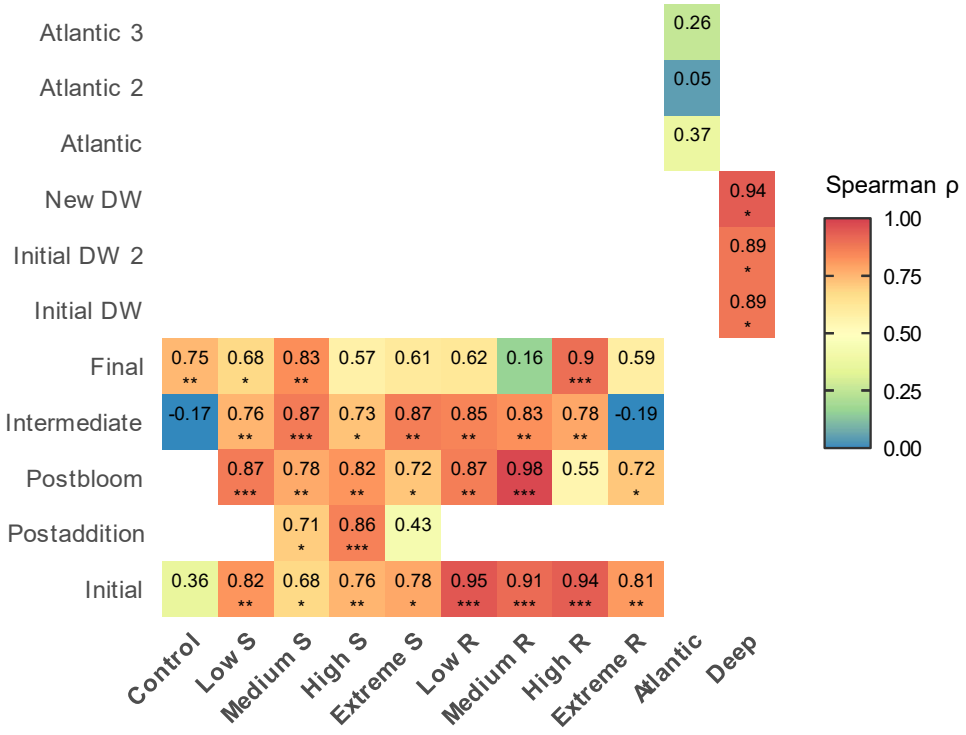

Fig. S12. Correlations between the cluster centroids of analogous clusters in the 0.2 µm and 3.0 µm size fractions. Asterisks denote the significance of the results: $p < 0.05$ (*), $p < 0.01$ (**) and $p < 0.001$ (***). ↺

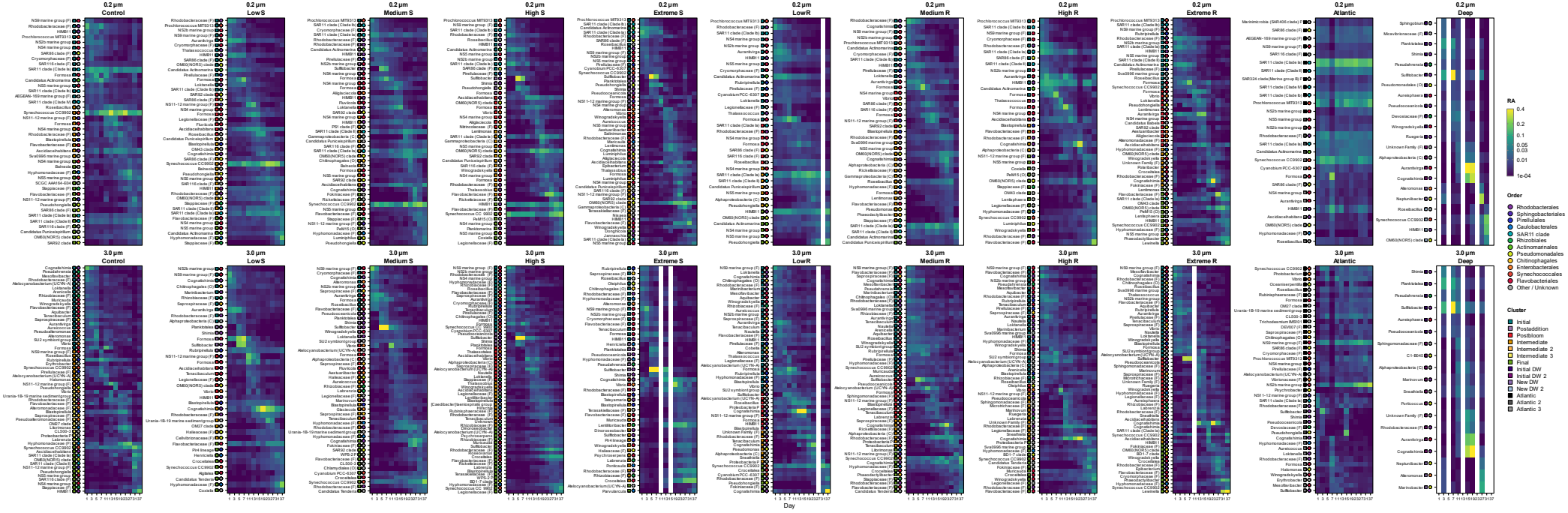

Figure S13. Succession patterns of most relevant prokaryotic taxa. Results are shown per treatment and size fraction as indicated on top of each panel. For each treatment and size fraction, ASVs with a membership value over 0.75 were merged by genera (when possible; otherwise, at the most detailed taxonomic level available, as indicated next to their name: F = family, O = order, C = class). From those, taxa representing at least 0.5% of reads in more than 1 sample within each treatment and size fraction are shown. Colourmap represents relative abundance (RA) of taxa (note that to aid visualisation 1) the scale is square−root−transformed and 2) out of bounds outlier values have been assigned the colours of the upper and lower limits of the colourmap). Coloured dots represent the taxonomic order of taxa, and cluster assignations are displayed next to taxa names. ↺

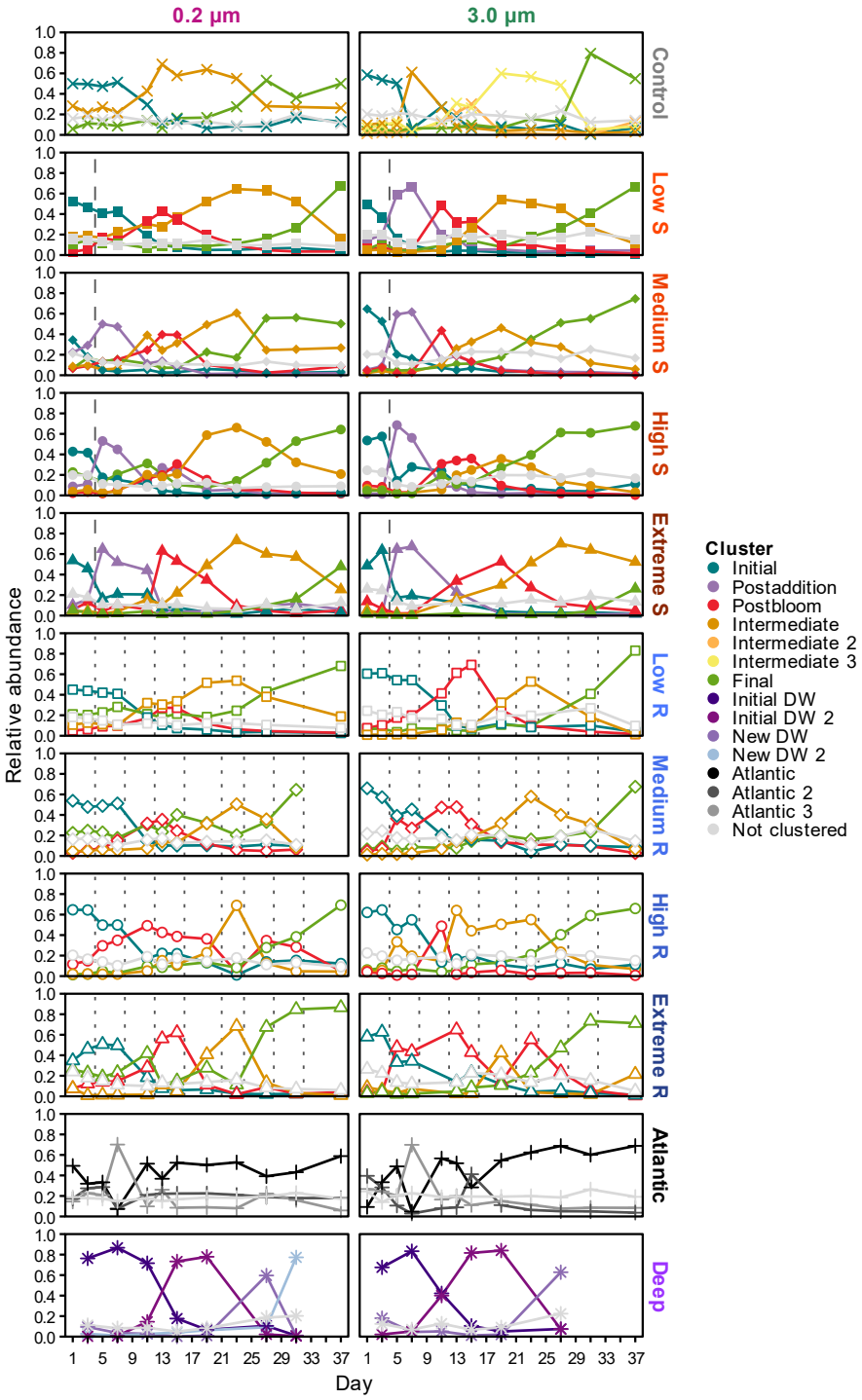

Figure S14. Relative abundance of ASVs contributing to each cluster. ASVs that were not included in the clustering (i.e., not exceeding >0.1% in any sample) are represented as 'Not clustered'. ↺

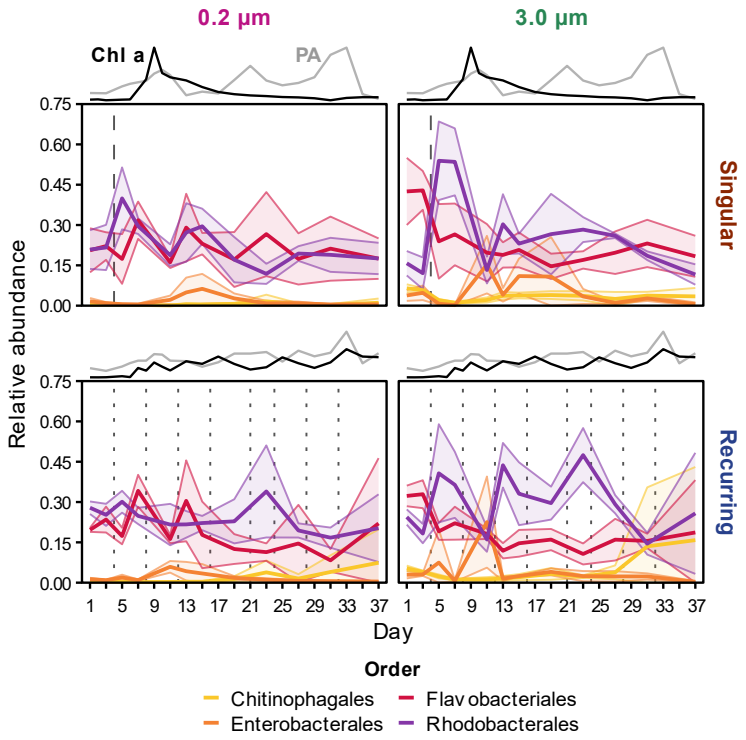

Fig. S15. Combined relative abundance of ASVs assigned to major orders associated with DOM cycling during blooms, averaged per upwelling mode (singular = upper row; recurring = lower row) and size fraction (0.2 µm = left column; 3.0 µm = right column). The shaded area around lines represents the ± standard deviation of averaged values for the different intensity treatments. Lines on top of plots show scaled Chl *a* (black) and prokaryotic abundance (PA, grey) values from Extreme treatments, in arbitrary units. Deep water additions are shown as dashed (singular) and dotted lines (recurring). ↺

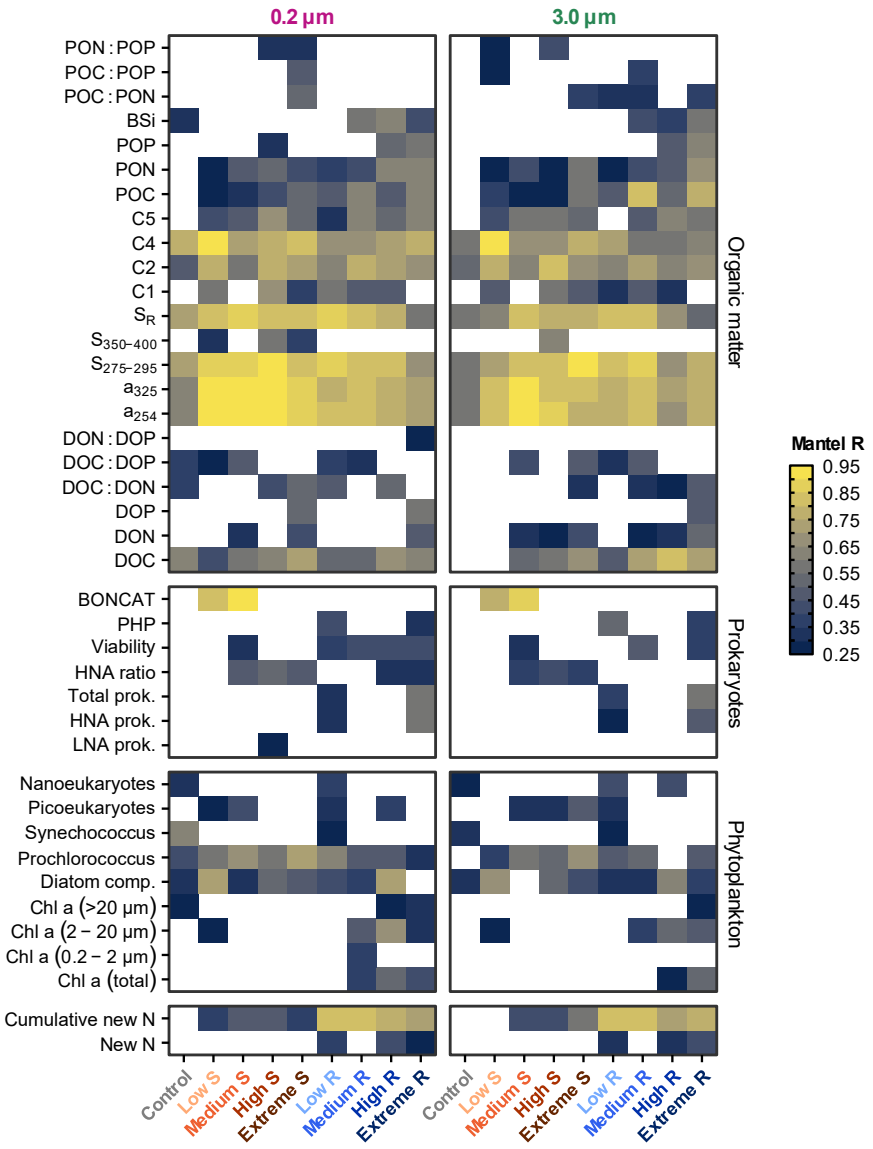

Figure S16. Relationship between prokaryotic community composition and biogeochemical parameters. For each treatment and size fraction, results of Mantel tests (*mantel* function, *vegan* (Legendre and Legendre 2012)) between sample dissimilarity matrices (Euclidean distances) based on 1) the CLR-transformed ASV abundance table and 2) the individual biogeochemical parameters are shown. Mantel tests were run with the Spearman method based on 9999 permutations. Only values of significant ($p < 0.05$) results are displayed. POC, PON and POP correspond to particulate organic carbon, nitrogen and phosphorus, respectively (Baumann et al. 2021); DOC, DON and DOP correspond to dissolved organic carbon, nitrogen and phosphorus, respectively. Their ratios are denoted with a ":". BSi corresponds to biogenic silica. a_{254}, a_{325} are absorption coefficients at 254 and 325 nm, respectively, while $S_{275-295}$ and $S_{350-400}$ are spectral slopes at those wavelength ranges, S_R being their ratio (Gómez-Letona et al. 2022). C1 and C5 are amino acid-like FDOM components, and C2 and C4 humic-like FDOM components (Gómez-Letona et al. 2022). Increases in a_{254} and a_{325}, decreases in $S_{275-295}$ and increases in humic-like fluorescence were suggested to indicate prokaryotic DOM transformation and increased recalcitrance (Gómez-Letona et al. 2022). See main text for a description of the parameters related to prokaryotes. Nanoeukaryotes, Picoeukaryotes, Prochlorococcus and Synechococcus refer to abundances of these groups as determined by flow cytometry. New N refers to the nitrogen introduced by deep water additions (including the cumulative values). Diatom comp. corresponds to the abundance-based diatom composition (Ortiz et al. 2022), for which dissimilarities were estimated based on the CLR-transformed abundance table. ↺

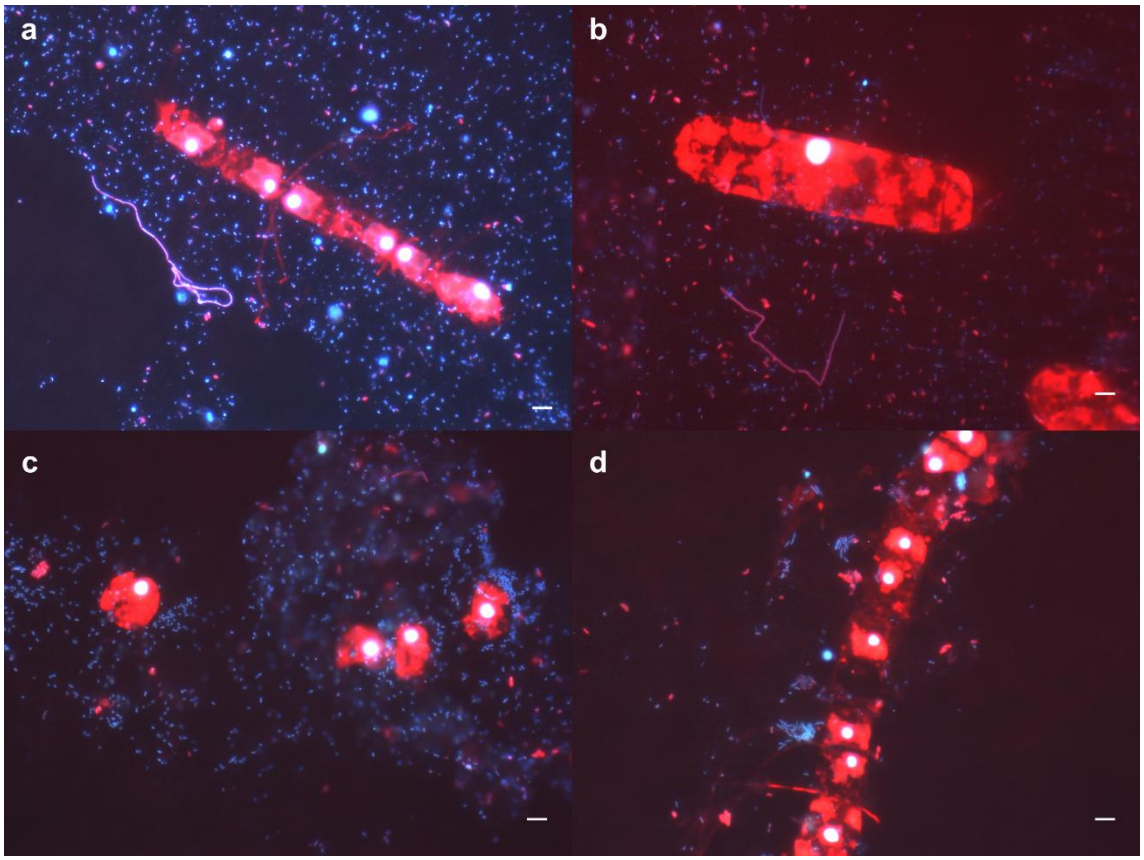

Figure S17. Examples of active eukaryotic phytoplankton. Images show the combined signal of 4′,6-diamidino-2-phenylindole (DAPI; all cells, blue) and Alexa594 (BONCAT+, protein-synthesising cells, red). a) Extreme S (day 9), b) Extreme R (day 13), c) Extreme S (day 13), and d) Extreme S (day 13). Scale bars (bottom right of each panel) represent 5 µm. ↺

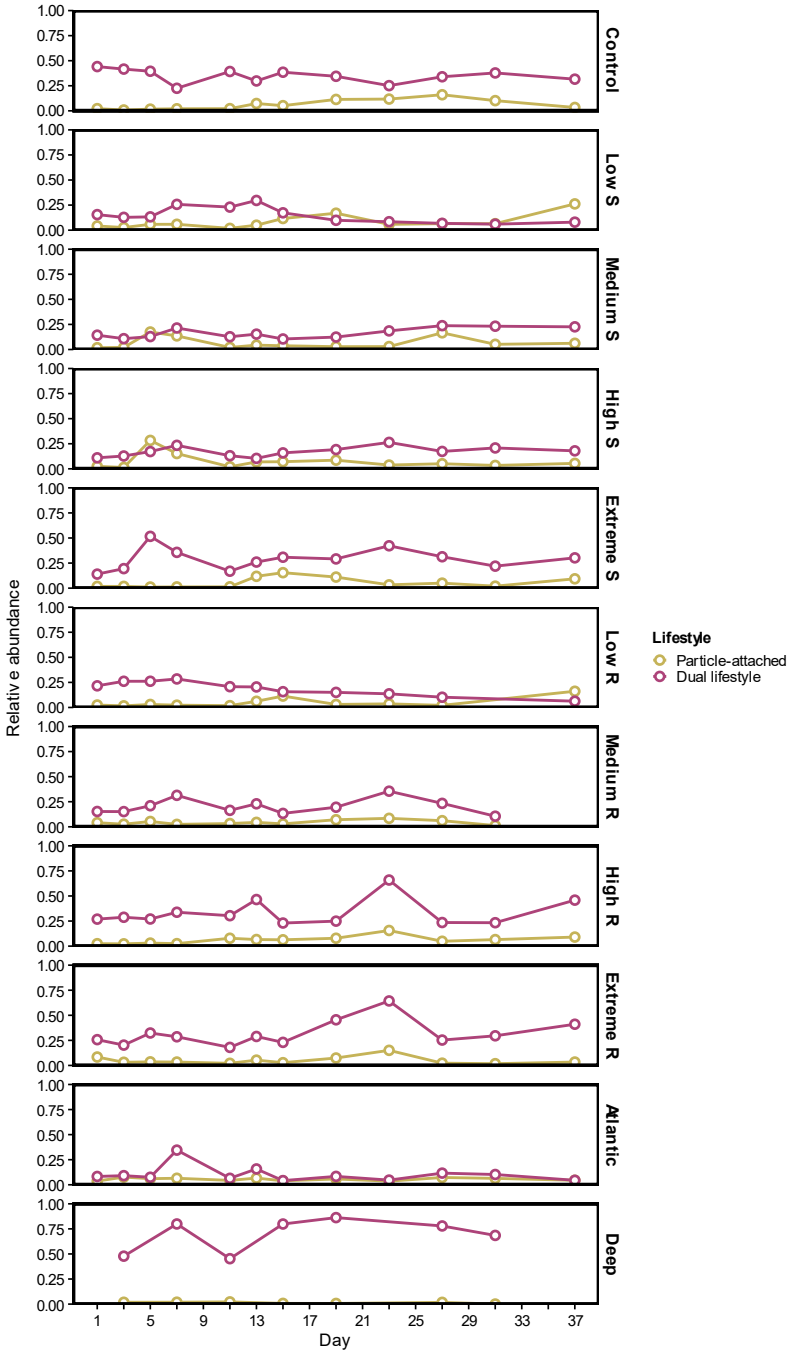

Fig S18. Contribution of ASVs with particle-attached and dual lifestyles to the free-living community (0.2 µm size fraction samples). ASV lifestyle was defined by means of differential abundance tests performed with the *corncob* package (v. 0.4.1, Martin et al. 2020): ASVs with particle-attached lifestyle were defined as those that were differentially more abundant in the 3.0 µm size fraction samples; free-living ones as those that were differentially more abundant in the 0.2 µm size fraction samples; and dual lifestyle ASVs were those which yielded non-significant results ($p \geq 0.05$) in the tests. See Sebastián et al. (2024) for more details on the ASVs categorisation. Tests were performed separately for each mesocosm, ambient waters and deep waters, controlling for the effect of *Day* on abundance. The contribution of the ASVs with particle-attached and dual lifestyles to the free-living community was quantified as the sum of the relative abundance of those ASVs in the 0.2 µm size fraction samples. ↺

References

Acinas, S. G., I. Ferrera, H. Sarmento, and others. 2015. Validation of a new catalysed reporter deposition–fluorescence in situ hybridization probe for the accurate quantification of marine Bacteroidetes populations. Environ. Microbiol. **17**: 3557–3569. doi:10.1111/1462-2920.12517

Annelie, P., P. Jakob, S. Martha, and A. Rudolf. 2002. Identification of DNA-Synthesizing Bacterial Cells in Coastal North Sea Plankton. Appl. Environ. Microbiol. **68**: 5728–5736. doi:10.1128/AEM.68.11.5728-5736.2002

Baumann, M., J. Taucher, A. J. Paul, and others. 2021. Effect of intensity and mode of artificial upwelling on particle flux and carbon export. Front. Mar. Sci. **8**: 742142. doi:10.3389/fmars.2021.742142

Catalá, T. S., A. M. Martínez-Pérez, M. Nieto-Cid, and others. 2018. Dissolved Organic Matter (DOM) in the open Mediterranean Sea. I. Basin–wide distribution and drivers of chromophoric DOM. Prog. Oceanogr. **165**: 35–51. doi:10.1016/j.pocean.2018.05.002

Catalá, T. S., I. Reche, M. Álvarez, and others. 2015. Water mass age and aging driving chromophoric dissolved organic matter in the dark global ocean. Global Biogeochem. Cycles **29**: 917–934. doi:10.1002/2014GB005048

Catalá, T. S., I. Reche, C. L. Ramón, À. López-Sanz, M. Álvarez, E. Calvo, and X. A. Álvarez-Salgado. 2016. Chromophoric signatures of microbial by-products in the dark ocean. Geophys. Res. Lett. **43**: 7639–7648. doi:10.1002/2016GL069878

Gómez-Letona, M., M. Sebastián, I. Baños, M. F. Montero, C. P. Barrancos, M. Baumann, U. Riebesell, and J. Arístegui. 2022. The importance of the dissolved organic matter pool for the carbon sequestration potential of artificial upwelling. Front. Mar. Sci. **9**: 969714. doi:10.3389/fmars.2022.969714

Hansen, H. P., and F. Koroleff. 1999. Determination of nutrients, p. 159–228. *In* K. Grasshoff, K. Kremling, and M. Ehrhardt [eds.], Methods of Seawater Analysis. Wiley Verlag Chemie GmbH.

Helms, J. R., A. Stubbins, E. M. Perdue, N. W. Green, H. Chen, and K. Mopper. 2013. Photochemical bleaching of oceanic dissolved organic matter and its effect on absorption spectral slope and fluorescence. Mar. Chem. **155**: 81–91. doi:10.1016/j.marchem.2013.05.015

Helms, J. R., A. Stubbins, J. D. Ritchie, E. C. Minor, D. J. Kieber, and K. Mopper. 2008. Absorption spectral slopes and slope ratios as indicators of molecular weight, source, and photobleaching of chromophoric dissolved organic matter. Limnol. Oceanogr. **53**: 955–969. doi:10.4319/lo.2008.53.3.0955

Kirchman, D. L. 1993. Leucine Incorporation as a Measure of Biomass Production by Heterotrophic Bacteria, p. 509–512. *In* P.F. Kemp, B.F. Sherr, E.B. Sherr, and J.J. Cole [eds.], Handbook of Methods in Aquatic Microbial Ecology. CRC Press.

Lawaetz, A. J., and C. A. Stedmon. 2009. Fluorescence intensity calibration using the Raman scatter peak of water. Appl. Spectrosc. **63**: 936–940. doi:10.1366/000370209788964548

Legendre, P., and L. Legendre. 2012. Numerical Ecology, Elsevier.

Leizeaga, A., M. Estrany, I. Forn, and M. Sebastián. 2017. Using click-chemistry for visualizing in situ changes of translational activity in planktonic marine bacteria. Front. Microbiol. **8**: 2360. doi:10.3389/fmicb.2017.02360

Lønborg, C., and X. A. Álvarez-Salgado. 2014. Tracing dissolved organic matter cycling in the eastern boundary of the temperate North Atlantic using absorption and fluorescence spectroscopy. Deep Sea Res. Part I Oceanogr. Res. Pap. **85**: 35–46. doi:10.1016/j.dsr.2013.11.002

Manz, W., R. Amann, W. Ludwig, M. Vancanneyt, and K.-H. Schleifer. 1996. Application of a suite of 16S rRNA-specific oligonucleotide probes designed to investigate bacteria of the phylum cytophaga-flavobacter-bacteroides in the natural environment. Microbiology **142**: 1097–1106. doi:10.1099/13500872-142-5-1097

Martin, B. D., D. Witten, and A. D. Willis. 2020. Modeling microbial abundances and dysbiosis with beta-binomial regression. Ann. Appl. Stat. **14**: 94–115. doi:10.1214/19-AOAS1283

Ortiz, J., J. Arístegui, J. Taucher, and U. Riebesell. 2022. Artificial upwelling in singular and recurring mode: consequences for net community production and metabolic balance. Front. Mar. Sci. **8**: 743105. doi:10.3389/fmars.2021.743105

R Core Team. 2021. R: A language and environment for statistical computing. R Foundation for Statistical Computing, Vienna, Austria. URL https://www.R-project.org/.

Sebastián, M., P. Sánchez, G. Salazar, and others. 2024. Water aging and the quality of organic carbon sources drive niche partitioning of the active bathypelagic prokaryotic microbiome. Limnol. Oceanogr. **69**: 562–575. doi:https://doi.org/10.1002/lno.12505

Sekar, R., A. Pernthaler, J. Pernthaler, F. Warnecke, T. Posch, and R. Amann. 2003. An Improved Protocol for Quantification of Freshwater Actinobacteria by Fluorescence In Situ Hybridization. Appl. Environ. Microbiol. **69**: 2928–2935. doi:10.1128/AEM.69.5.2928-2935.2003

Sharp, J. H. 1974. Improved analysis for “particulate” organic carbon and nitrogen from seawater1. Limnol. Oceanogr. **19**: 984–989. doi:https://doi.org/10.4319/lo.1974.19.6.0984

Sharp, J. H., E. T. Peltzer, M. J. Alperin, and others. 1993. Procedures subgroup report. Mar. Chem. **41**: 37–49. doi:10.1016/0304-4203(93)90104-V

Smith, D., and F. Azam. 1992. A simple, economical method for measuring bacterial protein synthesis rates in seawater using. Mar. Microb. food webs **6**: 107–114.

Stedmon, C. A., and R. Bro. 2008. Characterizing dissolved organic matter fluorescence with parallel factor analysis: A tutorial. Limnol. Oceanogr. Methods **6**: 572–579. doi:10.4319/lom.2008.6.572

Thomas, C., G. Cauwet, and J.-F. Minster. 1995. Dissolved organic carbon in the equatorial Atlantic Ocean. Mar. Chem. **49**: 155–169. doi:10.1016/0304-4203(94)00061-H

Utermöhl, H. 1931. Neue Wege in der quantitativen Erfassung des Plankton.(Mit besonderer Berücksichtigung des Ultraplanktons.). SIL Proceedings, 1922-2010 **5**: 567–596. doi:10.1080/03680770.1931.11898492

Welschmeyer, N. A. 1994. Fluorometric analysis of chlorophyll chlorophyll b and pheopigments. Limnol. Oceanogr. **39**: 1985–1992.